EUROPEAN ORGANIZATION FOR NUCLEAR RESEARCH

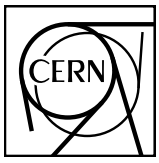

ALICE-ANA-2014-xxx
December 14, 2018

Hypertriton and anti-hypertriton production in the 2 body decay in Pb–Pb collisions at $\sqrt{s_{\rm NN}}$ = 5.02 TeV

Stefano Trogolo[1,2], Stefania Bufalino[2,3], Elena Botta[1,2]

1. Università degli Studi di Torino
2. INFN - Torino
3. Politecnico di Torino

Email: alice-analysis-hypertriton@cern.ch

Abstract

In this analysis note the details and results of the analysis on the ${}^{3}_{\Lambda}\mathrm{H}$ and ${}^{3}_{\Lambda}\overline{\mathrm{H}}$ production, perfomed on the data collected during 2015 Pb–Pb collisions at $\sqrt{s_{\rm NN}}$ = 5.02 TeV, are presented. The main goals of the present analysis are the measurement of the of ${}^{3}_{\Lambda}\mathrm{H}$ and ${}^{3}_{\Lambda}\overline{\mathrm{H}}$ production spectra and their lifetime at higher energy and with increased statistics with respect to the previous analysis performed on data collected during 2011 Pb–Pb collisions at $\sqrt{s_{\rm NN}}$ = 2.76 TeV [1]. The lifetime τ is estimated with two different approaches, the "corrected ct yields" and the "unbinned data fit", which lead to $\tau = 242^{+34}_{-38}$ (stat.) $\pm$ 20 (syst.) ps and $\tau = 240^{+40}_{-31}$ (stat.) $\pm$ 22 (syst.) ps, respectively.

Contents

1 Introduction

The hypertriton ($^3_\Lambda$H) is the lightest known hypernucleus and is formed by a proton, a neutron and a Λ baryon. $^3_\Lambda$H mesonic charged decay channels are:

$$^3_\Lambda\mathrm{H} \rightarrow ^3\mathrm{He} + \pi^- \quad (1)$$

$$^3_\Lambda\mathrm{H} \rightarrow \mathrm{d} + \mathrm{p} + \pi^- \quad (2)$$

$$^3_\Lambda\mathrm{H} \rightarrow \mathrm{p} + \mathrm{n} + \mathrm{p} + \pi^- \quad (3)$$

and their charge coniugate.

In this analysis note, we present the details of the analysis technique used to extract the production yields and the lifetime of $^3_\Lambda$H and $^{\overline{3}}_{\overline{\Lambda}}\overline{\mathrm{H}}$ in the 2 body decay channel (1) in Pb–Pb collisions at $\sqrt{s_{\mathrm{NN}}} = 5.02$ TeV. In particular, we will present two methods for the estimate of lifetime value: the "corrected yields" method and the "unbinned fit" method, which will be described later. All these results are compared to those previously obtained on 2011 data sample [1].

2 Data sample

2.1 Data

The analysis was performed on the Pb–Pb data sample collected during *LHC15o* period. The data sets used in this analysis are those at low Interaction Rate (lowIR) and high Interaction Rate (highIR), with full and reduced TPC acceptance. The *LHC15o* runlists used are the following:

LHC15o_highIR_pass1

- *DPG_CentralBarrelTracking_20161130_v6*: 246994, 246991, 246989, 246984, 246982, 246980, 246948, 246945, 246928, 246851, 246847, 246846, 246845, 246844, 246810, 246809, 246808, 246807, 246805, 246804, 246766, 246765, 246763, 246760, 246759, 246758, 246757, 246751, 246750, 246495, 246493, 246488, 246487, 246434, 246431, 246428, 246424, 246276, 246275, 246272, 246271, 246225, 246222, 246217, 246185, 246182, 246181, 246180, 246178, 246153, 246152, 246151, 246148, 246115, 246113, 246089, 246087, 246053, 246052, 246049, 246048, 246042, 246037, 246036, 246012, 246003, 246001, 245963, 245954, 245952, 245949, 245923, 245833, 245831, 245829, 245705, 245702, 245700, 245692, 245683

- *DPG_CentralBarrelTracking_TPCreduced_20161221_v6*: 246871, 246870, 246867, 246865, 246676, 246675

LHC15o_highIR_pass1_pidfix

- *DPG_CentralBarrelTracking_20161018_v0*: 245232, 245231, 245152, 245151, 245146, 245145

- *DPG_CentralBarrelTracking_TPCreduced_20161221_v0*: 245554, 245545, 245544, 245543, 245542, 245540, 245535, 245507, 245505, 245504, 245501, 245497, 245496, 245454, 245452, 245450, 245446, 245441, 245439, 245411, 245409, 245407, 245401, 245397, 245396, 245353, 245349, 245347, 245346, 245345, 245343, 245259

LHC15o_lowIR_pass3_pidfix

- *DPG_CentralBarrelTracking_20161109_v0*: 244918, 244975, 244980, 244982, 244983, 245064, 245066, 245068, 246390, 246391, 246392

2.2 Monte Carlo

The Monte Carlo data were used to study the cuts applied in the analysis of real data as well as for the efficiency × acceptance correction. A dedicated MC production - *LHC16h7{a,b,c}* - with injected signals and anchored to *LHC15o* runs was used, since the (anti-)hypertritons are not generated by HIJING.

The configuration of the MC is the following:

- **LHC16h7**: MC PbPb 2015, (anti-)nuclei and (anti-)hypernuclei injection, anchored to LHC15o
- Generator: HIJING
- Centrality range: 0–10% (*LHC16h7a*); 10–50% (*LHC16h7b*); 50–90% (*LHC16h7c*)
- Statistics:
  - 1.12×10^5 events generated in 0–10% (*LHC16h7a*);
  - 4.39×10^5 events generated in 10–50% (*LHC16h7b*);
  - 3.55×10^5 events generated in 50–90% (*LHC16h7c*);
- Injected signal per event:
  - flat injection in p_{T} ($0 \leq p_{\mathrm{T}} \leq 10$ GeV/c), y ($|y| < 1$) and ϕ ($0 \leq \phi < 2\pi$)
  - nuclei (d, t, ^3He, ^4He): 10 (Matter) + 10 (Antimatter);
  - $^3_\Lambda$H: 40 (Matter) + 40 (Antimatter), B.R. (^{3}He + π) = 50%, B.R. (d + p + π) = 50%;
  - $^4_\Lambda$H: 20 (Matter) + 20 (Antimatter), B.R. (^{4}He + π) = 50%, B.R. (t + p + π) = 50%;
  - $^4_\Lambda$He: 20 (Matter) + 20 (Antimatter), B.R. (^{3}He + p + π) = 100%

This MC production was done using the *AliDPG* [2] package, where all the configurations have been set in the PWGLF custom generators `Hijing_Nuclex004.C`

3 Event and Track selections

3.1 Event selection

The events used in this analysis are selected with the `"StandardLHC15oEventCuts"` implemented in `AliEventCuts` class and with a selection on the collision centrality, which is estimated using the V0M estimator (shown in Fig.1).

Event selection	
Centrality	0–90%
Trigger	`kINT7`
$\lvert z \rvert$ primary vertex	< 10 cm
z_{SPD} vertex resolution	< 0.25 cm
$\lvert z_{SPD} - z_{Track} \rvert$ vertex	< 0.2 cm
$\mathrm{n}\sigma_{SPD}\ \Delta^{vertex}_{SPD-Track}$	< 10
$\mathrm{n}\sigma_{Track}\ \Delta^{vertex}_{SPD-Track}$	< 20

Table 1: Cuts used to selected events

Pile-up rejection SPD	
Number of contributors	> 5
z distance from primary vtx	> 0.8 cm
$\mathrm{n}\sigma_z$ distance from primary vtx	> 3
$\mathrm{n}\sigma_z$ diamond zone	< 5
$\mathrm{n}\sigma_{xy}$ diamond zone	< 2

Table 2: Cuts used to reject pile-up vertices

The cuts used to select the events used in this analysis are listed in Table 1, while those applied for the rejection of pileup vertices with SPD are listed in Table 2. More details on the pileup vertex rejection can be found looking the method `IsPileUpFromSPD` in `AliRoot/STEER/ESD/AliESDEvent.cxx`.

The total number of events which satisfied these selections and were used in this analysis is 104.8×10^6.

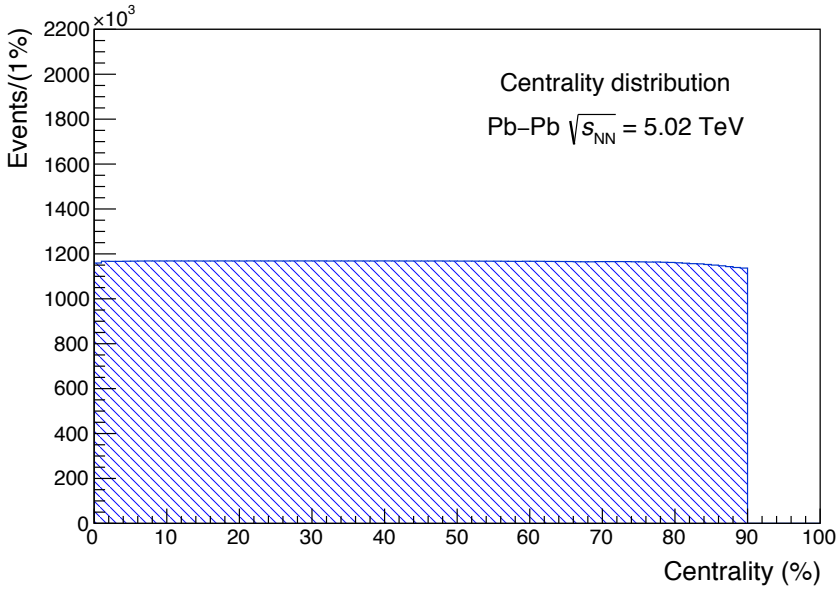

Fig. 1: Centrality distribution of *LHC15o* using V0M estimator

3.2 Track selection

The candidate tracks, used to reconstruct the ${}^{3}_{\Lambda}\mathrm{H}$ and ${}^{3}_{\bar{\Lambda}}\overline{\mathrm{H}}$ decay, are required to satisfy the selections listed in Table 3.

Track cuts	
$\mid \eta \mid$	< 0.9
TPC clusters	> 80
χ^2 per TPC clusters	< 5
TPC refit	TRUE
Kink daughters	reject

Table 3: Cuts used to select candidate tracks

4 Analysis Technique

4.1 Particle IDentification

The ALICE detector used to identify the candidate ^{3}He and π in this analysis, is the Time Projection Chamber (TPC). Particles, passing through the detector, are identified via their specific energy loss (dE/dx) in the TPC gas. The measured dE/dx value is compared with the value of Bethe-Bloch function which gives the expected energy loss, given the particle species and the momentum.

Fig.2 and 3 show the measured specific energy loss (dE/dx) versus rigidity p/Z in Pb–Pb collisions at 5.02 TeV , where p is the track momentum at the inner wall of TPC (`esdtrack` $\rightarrow$ `GetInnerParam` $\rightarrow$ `GetP`) and Z is the charge of the species The superimposed red lines are the Bethe-Bloch curves parameterized with TSplines within the AliRoot framework, which are obtained with fits to real data using pure PID sample. These parameterizations are used for the identification of the candidate ^{3}He and π. If the energy loss of a certain track lies within a certain number of σ's from the expected value of the Bethe-Bloch for a certain particle, the track is identified with that particle species. σ is the resolution on the specific energy loss measured in TPC, which is $\approx 6\%$.

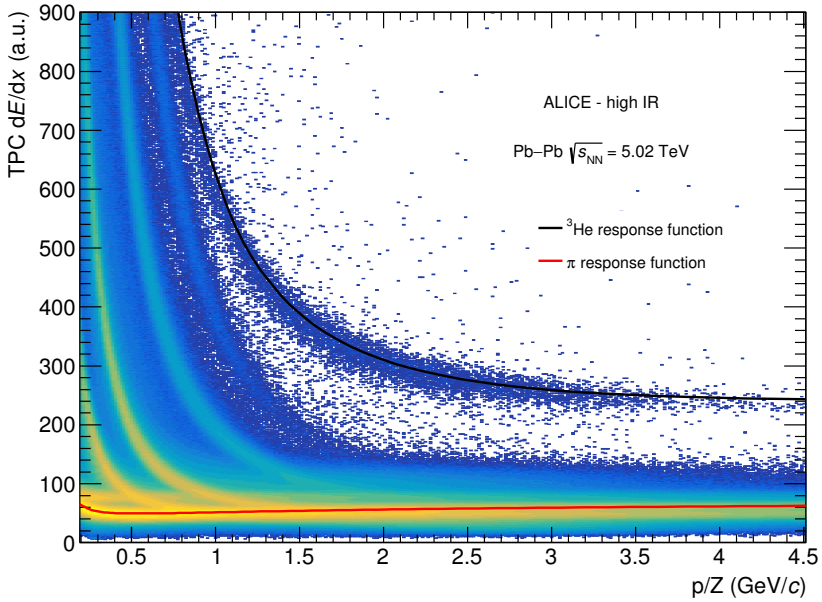

Fig. 2: TPC energy loss in high IR Pb–Pb at 5.02 TeV, with superimposed the TSplines parameterization used for the PID in this analysis.

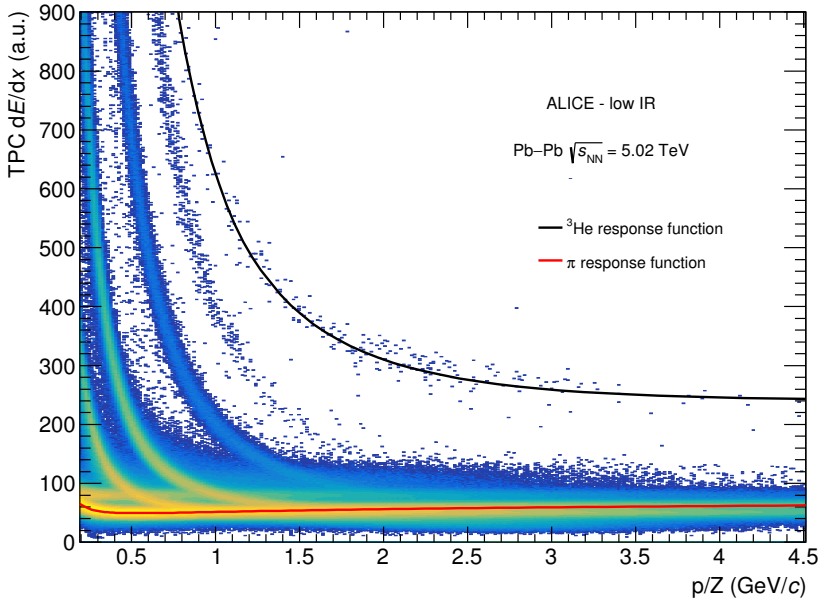

Fig. 3: TPC energy loss in low IR Pb–Pb at 5.02 TeV, with superimposed the TSplines parameterization used for the PID in this analysis.

Pions and ^{3}He are identified applying a 3σ cut on the difference between measured and expected dE/dx. Since the ^{3}He energy loss in the TPC is very close to that of triton, the candidate ^{3}He tracks are required to be away by at least 0 sigma from the triton band ($n\sigma_{triton} > 0$). In Table 4 are reported the nσ cuts used for the particle identification in this analysis.

Particle IDentification	
π	$\mid n\sigma \mid < 3$
^{3}He	$\mid n\sigma \mid < 3$ $n\sigma_{triton} > 0$

Table 4: $n\sigma$ cuts used for the PID of the π and ^{3}He tracks.

4.2 Secondary vertex reconstruction

After the identification of the candidate daughters tracks, it is possible to proceed with the reconstruction of the hypertriton secondary vertex. In particular, in this analysis, the decay vertex is identified using the on-the-fly V^0-finder algorithm, which reconstructs the V^0 decay vertex during the data reconstruction phase. This algorithm has access to the local characteristics of the helix describing the trajectory and, in this way, it can include the material budget in the reconstruction of the particle trajectory, which is not available after reconstruction instead. The inclusion of the material budget is important because it allows to correct for particle energy loss in dead zones of the apparatus, leading to the correct momentum of the daughter tracks at the reconstructed decay vertex. This is extremely important for the ^{3}He, which has a substantial energy loss and must be corrected for it. The V^0-finder pairs a positive and a negative track and selects the V^0 candidate with a set of loose cuts, which are listed in Table 5. More details on the V^0-finder algorithm can be found in [3]

on-the-fly V^0 finder	
track $DCA_{primaryvtx}$	$>$ 1mm
DCA V^0 daughters	$<$ 1.5 cm
$\cos(\theta_{pointing})$	> 0.9

Table 5: V^0-finder loose cuts used to reconstruct and select V^0 candidate

5 $^3_\Lambda$H Lifetime determination

The increased statistics of 2015 Pb–Pb data taking period allow to determine the lifetime of the hypertriton with a better precision with respect to the previous result of $\tau = 181^{+54}_{-39}$(stat.)$\pm$ 33 (syst.) ps, obtained analysing the 2011 Pb–Pb data sample. For this analysis all the events with centrality in the range 0–90%and satisfying the event selection of Sec. 3.1, were used. Assuming that $^3_\Lambda$H and $^3_{\bar{\Lambda}}\overline{\mathrm{H}}$ have the same lifetime, it has been possible to analyse the sample obtained summing matter and antimatter candidates. Fig.4 shows a pictorical sketch of the $^3_\Lambda$H two body decay together with the topological observables used in the candidates selection and for the combinatorial background reduction.

The candidate daughters (π^-+^{3}He and π^++$^3\overline{\mathrm{He}}$) were identified applying the same criteria and cuts presented in Sec. 4.1. An additional set of topological and kinematic cuts was studied on the MC sample and applied to the data to further reduce the background and improve the signal extraction from the invariant mass distribution for $^3_\Lambda$H and $^3_{\bar{\Lambda}}\overline{\mathrm{H}}$ candidates. These cuts are listed in Table 6 and some of them have been changed with respect to the 2011 analysis. For example the $\cos(\theta_{pointing})$ which has been tighten or the rapidity y range which has been enlarged.

A huge discrepancy between $^3_\Lambda$H and $^3_{\bar{\Lambda}}\overline{\mathrm{H}}$ distributions was observed, leading to a Signal/Background (S/B) higher for the antimatter than for the matter. The discrepancy between matter and anti-matter is due to the fact that ^{3}He is produced by secondary interactions and, at the same time, the $^3\overline{\mathrm{He}}$ with similar momentum can be absorbed. In order to reject the ^{3}He from secondary interaction, the candidate nucleus was required to have p_{T} greater than 1.8 GeV/c.

As discussed in Sec.2.2, $^3_\Lambda$H and $^3_{\bar{\Lambda}}\overline{\mathrm{H}}$ were injected with a flat p_{T} distribution between 0 and 10 GeV/c

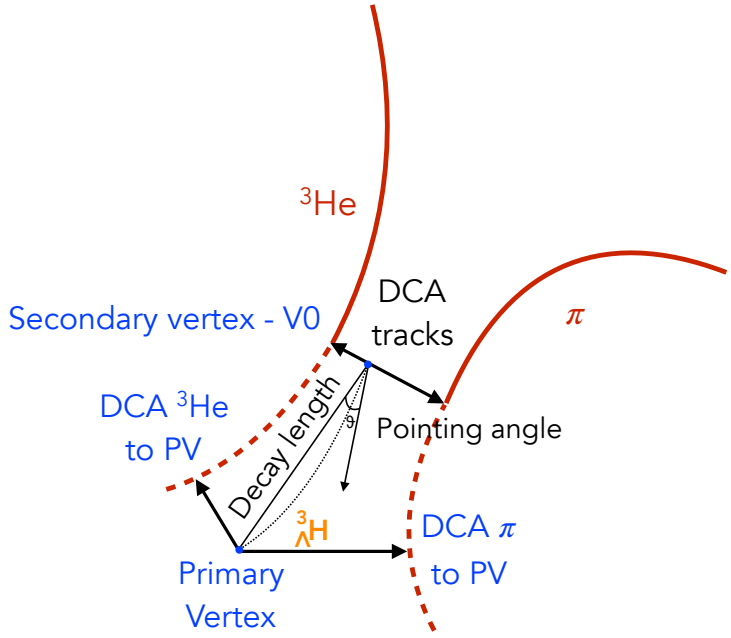

Fig. 4: Pictorical sketch of the $^3_\Lambda$H two body decay. The observables which have been used to reduce the combinatorial background are reported on the figure.

Cut	value
^{3}He p_{T}	1.8 ÷ 10 GeV/c
DCA$_{tracks}$	$<$ 0.7 cm
cos($\theta_{pointing}$)	$>$ 0.995
p_{T} mother	$>$ 2 GeV/c
p_{T} mother	$<$ 10 GeV/c
ML/p	$<$ 40 cm
ML/p	$>$ 0 cm
$\lvert y\rvert$	$<$ 0.8

Table 6: Cuts applied in this analysis to improve the signal extraction from the invariant mass distribution for the lifetime measurement

in the MC production. Looking at the p_{T} distribution of the true reconstructed $^3_\Lambda$H and $^3_\Lambda\overline{\mathrm{H}}$ in Fig.5, it is clearly visible that for p_{T} lower than 2 GeV/c few candidates are reconstructed. A cut on the minimum p_{T} at 2 GeV/c was applied to reduce the background from a p_{T} region with low signal reconstruction efficiency.

Other cuts applied for the signal extraction are the minimum cosine of the pointing angle (cos$\theta_{pointing}$), required to be larger than 0.995, which relates the $^3_\Lambda$H momentum and the vector connecting primary and secondary vertex, the maximum distance of closest approach (DCA$_{tracks}$) between the daughter tracks, lower than 0.7 cm, the rapidity of the reconstructed mother, which lies between -0.9 and 0.9. It was also added a selection on the decay length ct, which is required to vary between 0 and 40 cm.

The methods proposed and used for the lifetime determination in this analysis are two. The first one, described in Sec.5.1, is to divide the total ct distribution into six bins, extract the signal from the invariant mass distribution, correct for the efficiency $\times$ acceptance vs ct, and fit the corrected spectra with an

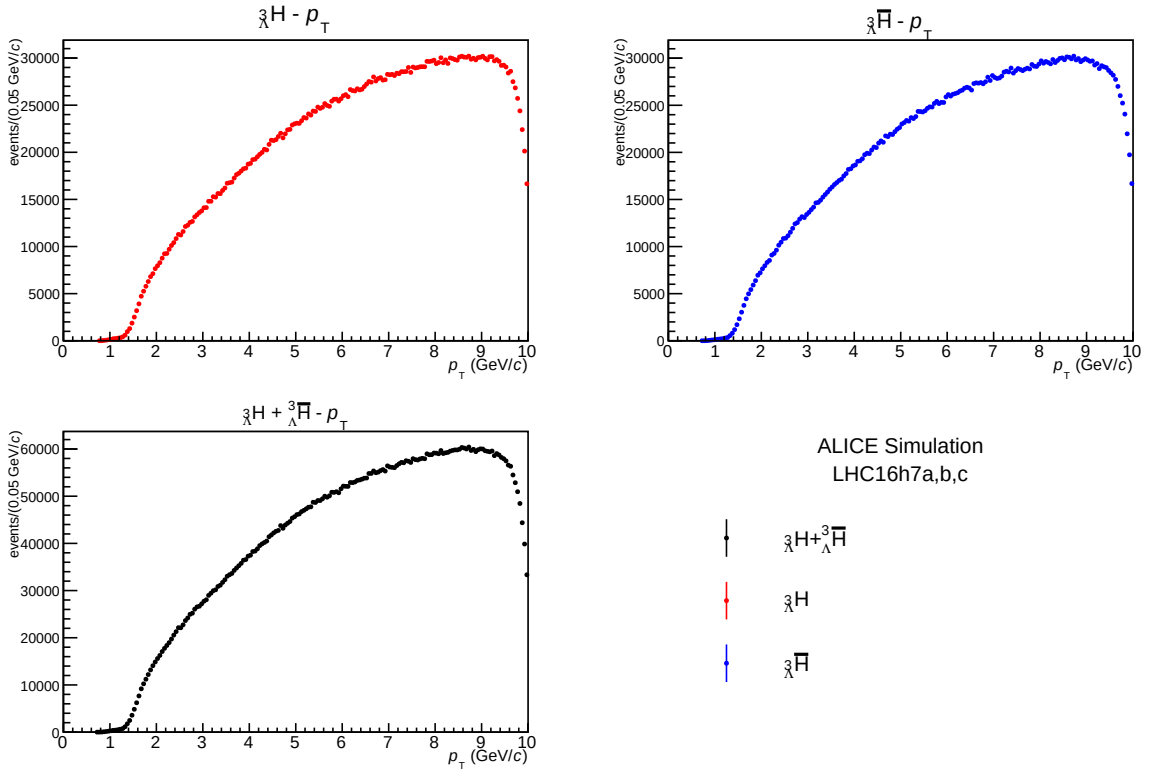

Fig. 5: p_{T} distribution obtained from MC *LHC16h7* of reconstructed and true $^3_\Lambda$H (left - red marker), $^3_\Lambda\overline{\text{H}}$ (middle - blue marker) and $^3_\Lambda$H + $^3_\Lambda\overline{\text{H}}$ (right - black marker)

exponential function:

$$N(t) = N_0 \cdot e^{-\frac{ct}{c\tau}} \tag{4}$$

The second method, reported in Sec.5.2, is to perform an unbinned 2-dimensional fit to the "invariant mass vs ct" distribution, using the maximum-likelihood estimate option to estimate the lifetime. This second method was done using the package RooFit in ROOT6.

The definition of ct is

$$ct = \frac{MLc}{p} \tag{5}$$

where M is the nominal value of the $^3_\Lambda$H mass of 2.991 GeV/c^2 [4], L is the measured decay distance and p is the total momentum of the $^3_\Lambda$H candidate. In particular, the decay distance is evaluated using this formula:

$$L = \sqrt{(\Delta_x)^2 + (\Delta_y)^2 + (\Delta_z)^2} \tag{6}$$

with

$$\Delta_x = x_{SV} - x_{PV} \quad \Delta_y = y_{SV} - y_{PV} \quad \Delta_z = z_{SV} - z_{PV} \tag{7}$$

where (x_{PV}, y_{PV}, z_{PV}) and (x_{SV}, y_{SV}, z_{SV}) are the primary and secondary vertex coordinates, respectively. For electrically neutral particles, the track length is the straight line distance between the production vertex and decay vertex. For charged particles produced in the collision passing through the ALICE detectors, the decay distance is equivalent to the helix segment length, because of the presence of the solenoidal magnetic field of L3. In this last case the definition of the length of the helix segment is:

$$\text{Helix length} = \sqrt{(\text{Ark length})^2 + (\Delta_z)^2} \tag{8}$$

with

$$\text{Ark length} = 2R \cdot arcsin\left(\sqrt{\frac{\Delta_x^2 + \Delta_y^2}{2R}}\right) \tag{9}$$

R is the curvature radius of the charged track, which is defined with the usual formula

$$R = \frac{p_T}{qB} = \frac{p_T}{B}\frac{10}{3} = 0.3 \cdot \frac{p_T}{B} \tag{10}$$

where the p_T is given in units of GeV/c, B in Tesla $\left[\frac{V \cdot s}{m^2}\right]$ and R in m.

From the comparison, already shown in [1], of the decay distance vs helix length for the ${}^3_\Lambda$H candidates with p_T within 2 ÷ 10 GeV/c, there are no visible differences. For this reason, in the following, the "decay distance" referes to Eq.6.

5.1 Corrected *c*t spectra method

5.1.1 Raw yields vs ct

The first step is to extract raw production yields in different ct bins. The ct range is divided in six bins (2-4, 4-7, 7-10, 10-15, 15-28, 28-40 cm). For each bin the signal is extracted performing a fit to the invariant mass distribution (π^-+^{3}He and π^++${}^3\overline{\text{He}}$) with a function which is the sum of a Pol2 (*background*) and a Gaussian (*signal*). Fig.6 shows the invariant mass spectrum obtained for six ct bins, with superimposed the fit function, used for the raw yields extraction, and the results of the fit.

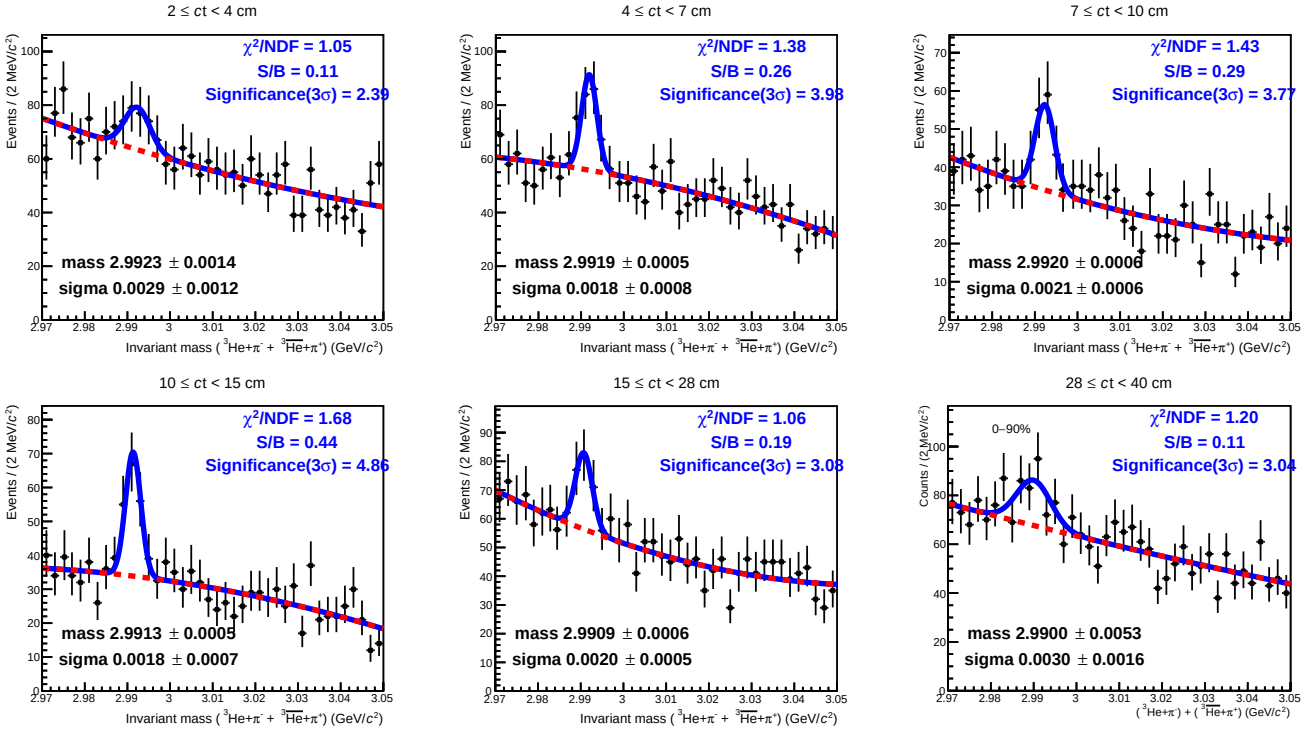

Fig. 6: (${}^3_\Lambda$H + ${}^3_{\overline{\Lambda}}\overline{\text{H}}$) invariant mass spectra for 6 ct bins, with superimposed the fit function (blue curve), used to extract the raw yields, and the background (red dashed curve).

The mass values obtained from the gaussian function used in the fit to the invariant mass was compared with the expected value of 2.99116 ± 0.00005 GeV/c^2, taken from [4]. In Fig.7 the red line is the expected value and the orange band is the related uncertainty. The blue markers are the mean value and

ct bin	**Raw yield** (3σ)
$2 \leq c\text{t} < 4$ cm	76 ± 24
$4 \leq c\text{t} < 7$ cm	73 ± 17
$7 \leq c\text{t} < 10$ cm	68 ± 13
$10 \leq c\text{t} < 15$ cm	80 ± 16
$15 \leq c\text{t} < 28$ cm	59 ± 16
$28 \leq c\text{t} < 40$ cm	54 ± 18

Table 7: Raw yields extracted in the six ct bins

the sigma of the gaussian, obtained in the different ct bins, and they are in agreement with the expected one.

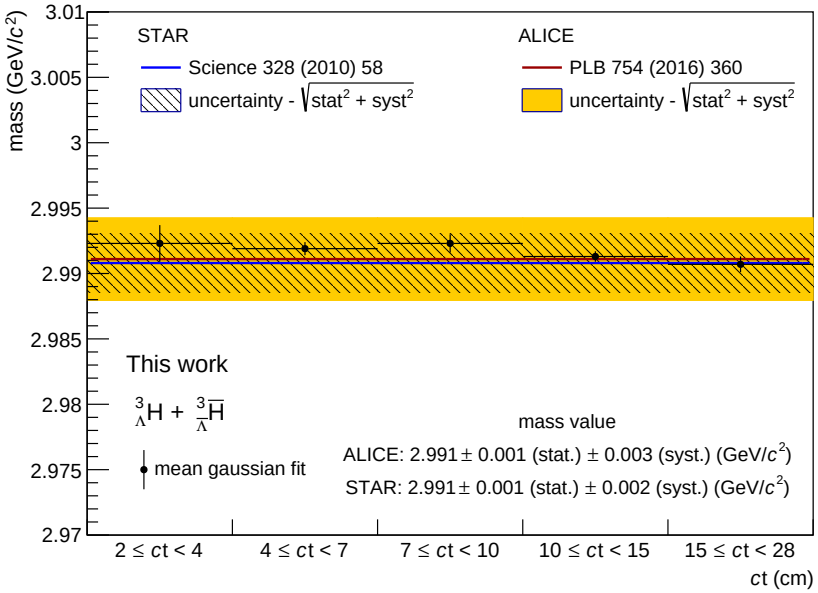

Fig. 7: Mass value obtained from the fit to the invariant mass distributions in the different ct bins (blue markers) compared with the expected value (red line) and its related uncertainty (orange band) from [4].

Table 7 shows the raw yields determined, in the different ct bins, as the integral of the Gaussian function in the region of $\pm\, 3\sigma$ w.r.t. the mean value (*mass*) obtained from the fit.

5.1.2 Efficiency vs ct

Measured raw yields are biased by the efficiency and acceptance of the ALICE detectors. The acceptance is related to the geometric coverage of the detectors. The efficiency, instead, is related to many sources (e.g. tracking algorithm, the experiment is not hermetic, detector parts switched off in data acquisition) which can affect the reconstruction.

It is possible to correct for this efficiency and acceptance using a MC simulation, where the geometry and detectors data taking conditions are reproduced. For the evaluation of the lifetime, the efficiency $\times$ acceptance is studied as a function of ct and can be defined as:

$$Efficiency \times Acceptance = \frac{N^{\text{rec}}(ct)}{N^{\text{gen}}(ct)} \tag{11}$$

where N^{rec} is the number of reconstructed and true ${}^{3}_{\Lambda}\text{H}$ (${}^{3}_{\bar{\Lambda}}\overline{\text{H}}$) satisfying the criteria summarised in Table 6 and N^{gen} is the number of ${}^{3}_{\Lambda}\text{H}$ (${}^{3}_{\bar{\Lambda}}\overline{\text{H}}$) generated in the same centrality range, in the azimuthal region 0

$\leq \phi < 2\pi$ and in the rapidity region $|y|< 0.8$. Moreover, the same PID criteria reported in Table 4 were required for the evaluation of $N^{\rm rec}$.

An important addition in the evaluation of $N^{\rm rec}$ is the correction for the absorption from material. The probability to observe an ${}^3_\Lambda$H ($p_{Observe_{{}^3_\Lambda{\rm H}}}$) is obtained as described in detail in Sec.6 and it is used to correct $N^{\rm rec}$. Since this probability is given as a function of $p_{\rm T}$ while the lifetime is obtained from a ct spectrum and there is not a correlation between $p_{\rm T}$ and ct, the correction was applied through a 2D histogram. First $N^{\rm rec}(p_{\rm T}$ and ct) was computed: a TH2F was filled with $N^{\rm rec}$ in each ($p_{\rm T}$, ct) cell, obtaining a map ($p_{\rm T}$ *vs* ct) of the number of reconstructed ${}^3_\Lambda$H and ${}^3_{\bar\Lambda}\overline{\rm H}$. Then the entries of each bin were corrected with the probability (orange histogram in Fig.16) of the corresponding $p_{\rm T}$ bin, $N^{\rm rec}(p_{\rm T}, c{\rm t}) \cdot p_{Observe_{{}^3_\Lambda{\rm H}}}(p_{\rm T})$. Finally $N^{\rm rec}$ as a function of ct was obtained by projecting the TH2F on the ct axis, from the first to the last $p_{\rm T}$ bin. This $N^{\rm rec}$ *vs* ct distribution was used to evaluate the efficiency $\times$ acceptance.

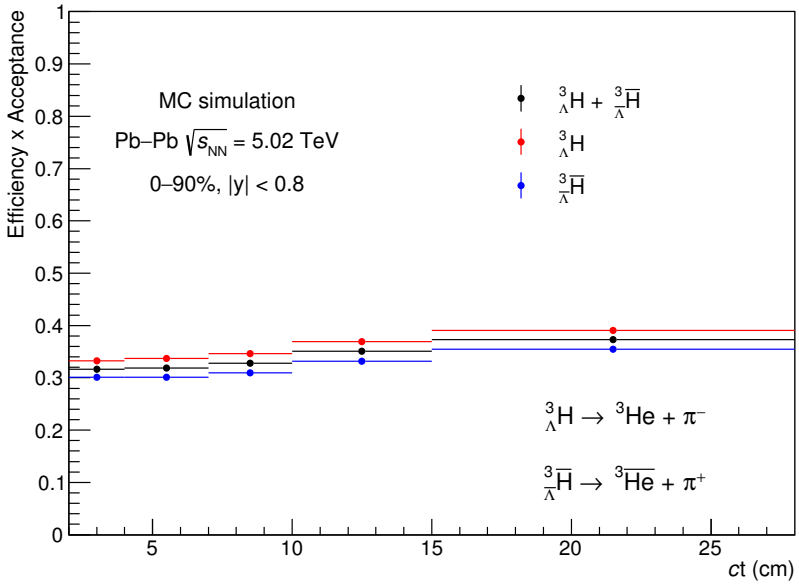

Fig. 8: Efficiency $\times$ acceptance vs ct for ${}^3_\Lambda$H (red), ${}^3_{\bar\Lambda}\overline{\rm H}$ (blue) and ${}^3_\Lambda$H + ${}^3_{\bar\Lambda}\overline{\rm H}$ (black). The same bins for the yields are used.

The efficiency $\times$ acceptance is computed using the same ct bins which are used to extract the raw yields. Fig.8 shows the efficiency $\times$ acceptance for ${}^3_\Lambda$H (red points) and ${}^3_{\bar\Lambda}\overline{\rm H}$ (blue points) separately, and for the sum (black points). The latter one is used to correct the raw yields in order to obtain the corrected dN/d(ct)spectrum.

5.1.3 Results

The first (2-4 cm) and the last (28-40 cm) ct bins have not been included in the final corrected spectrum. The reasons are the high background contamination, which do not allow to extract a clear signal and raw yield, and, for the first bin, the fact that the efficiency is obtained in the rising part of it, while for the other bins the efficiency is almost flat. Fig.9 shows the corrected yields, fitted with a TF1 exponential function. Performing the fit, the ROOT option "I" has been used and it uses the integral of the function in the full bin instead of the value at bin center.

The results from the fit are:

$$c\tau = 7.25^{+1.02}_{-1.13}(stat.)\ cm \tag{12}$$

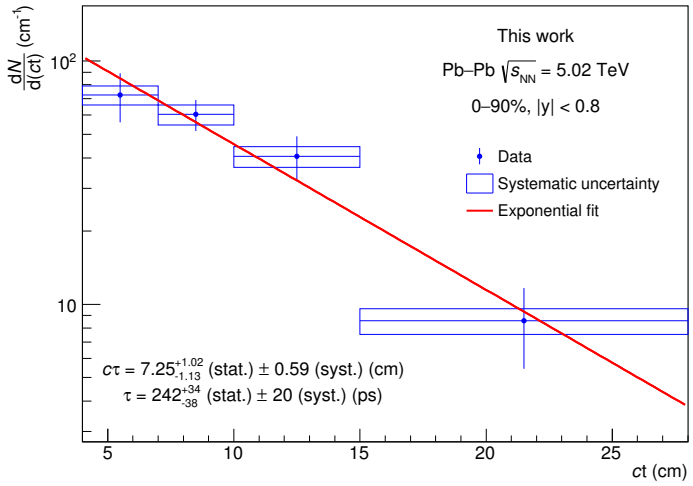

Fig. 9: Corrected yields vs ct (only stat. uncertainty). Points are fitted with an exponential function using the integral of the function in the full bin instead of the value at bin center.

$$\tau = 242^{+34}_{-38}(stat.)\ ps \tag{13}$$

5.2 Unbinned fit method

The second method consists of an unbinned maximum likelihood fit to the data of the ${}^{3}_{\Lambda}\mathrm{H}$ and ${}^{3}_{\bar{\Lambda}}\overline{\mathrm{H}}$ candidates, which have been selected with the selection criteria reported in Table 4 and 6. The procedure of this method can be divided in three steps:

- estimate of the signal (N_s, σ) and background (N_b) contribution to the invariant mass distributions;
- tuning the function for the uncorrelated ct background in the side-band regions;
- determination of the lifetime τ performing a fit in the signal with a proper pdf.

This method was tested re-performing the analysis on 2011 data sample by Lukas Kreis and the results found, which are in agreement with the published results [1], have been presented during the PAG NuclEx meeting of the 1st February 2017. [1]

5.2.1 Parameters estimate

In order to fit the ct distribution to estimate the lifetime, it was important to quantify the signal (N_s) and the background (N_b) counts in the signal region. This region is defined using the number of σ w.r.t. to the hypertriton mass value. These parameters were obtained from the invariant mass distribution of (π^-+^{3}He) and (π^++${}^3\overline{\mathrm{He}}$) candidates, which have been selected applying the set of cuts listed in Tables 4 and 6. The fit to the invariant mass distribution, integrated over the ct range (0-28 cm), was performed with a function which is the sum of a Gaussian (*signal*) and a Pol2 (*background*).

Fig.10 shows the invariant mass distribution, ct integrated, with superimposed the the total function (*blue line*), the pol2 for the background (*red dashed line*) and the gaussian for the signal (*black dashed line*). The mean value and the σ from the Gaussian are used to define the signal region (-3σ,+3σ) and the sidebands [(-9σ,-3σ) and (+3σ,+9σ)] used for the lifetime estimate. These regions are shown in Fig.10

[1] https://indico.cern.ch/event/609538/

with a central white (signal) and two red lined (sidebands) regions. The signal N_s and the background N_b counts are obtained from the maximum-likelihood estimate fit to the invariant mass distribution of the candidates. Then they are scaled to the signal region using the integral of the fit function within that region.

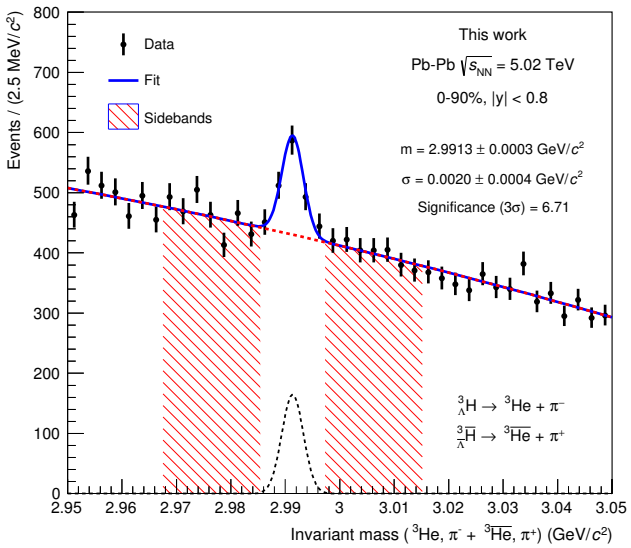

Fig. 10: ($^3_\Lambda$H + $^3_{\bar\Lambda}\bar{\text{H}}$) invariant mass distribution with superimposed the total function (*blue line*), the background (*red dashed line*) and the signal (*black dashed line*) components. Central white region is the signal range, while red lined regions are the sidebands.

5.2.2 *Background tuning*

The uncorrelated background in the ct distribution was considered before performing the fit in the signal region for the lifetime estimate. This background has been modeled with function which is the sum of two exponential pdfs:

$$pdf_{Bkg,1} = N_{\text{Bkg},1} \cdot e^{-\frac{ct}{\tau_{b1}}} \quad , \quad pdf_{Bkg,2} = N_{\text{Bkg},2} \cdot e^{-\frac{ct}{\tau_{b2}}} \tag{14}$$

where $N_{\text{Bkg},1}$ and $N_{\text{Bkg},2}$ are the normalization constants to take into account the background counts in the sidebands, while τ_{b1} and τ_{b2} are the time constants of the two exponential functions. The parameters, especially τ_{b1} and τ_{b2}, have been tuned with a fit to the sidebands. The result is shown in Fig.11, where the black histogram is the fit function.

5.2.3 *Results*

The lifetime estimate is done performing a fit to the ct distribution in the signal range. The function used for the fit is the sum of the two background exponentials, discussed in the previous section and normalized to the background counts in the signal range, and an exponential pdf for the signal. The exponential function used for the signal is the following:

$$pdf_{signal} = N_s \cdot e^{-\frac{ct}{c\tau}} \tag{15}$$

where τ is the $^3_\Lambda$H lifetime to be estimated and N_s is the signal counts obtained from the fit to the invariant mass and discussed in Sec.5.2.1. The signal pdf needs to be corrected to take into account the efficiency

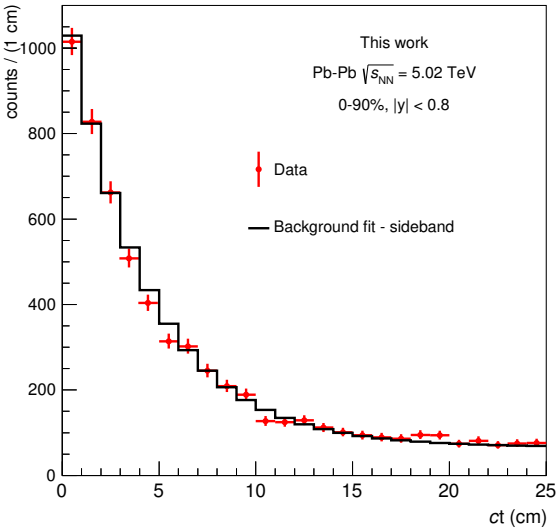

Fig. 11: ct distribution in the sidebands with superimposed the total fit function (black) which is the sum of two exponentials pdfs.

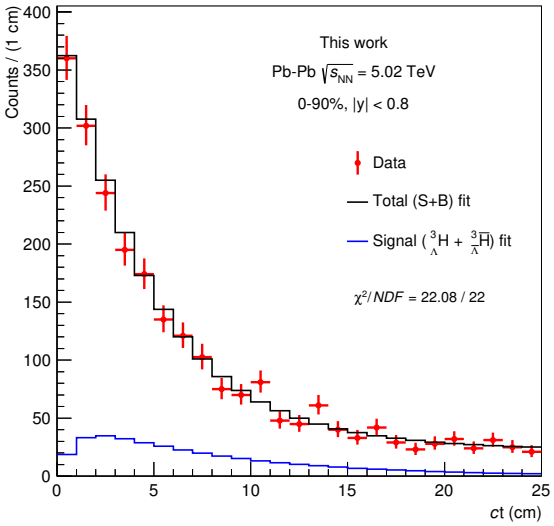

Fig. 12: ct distribution in the signal region with superimposed the total fit function (black) and exponential for $^{3}_{\Lambda}$H and $^{3}_{\bar{\Lambda}}\bar{\text{H}}$ lifetime (blue).

and acceptance of the detector. The efficiency $\times$ acceptance was computed for $^{3}_{\Lambda}$H and $^{3}_{\bar{\Lambda}}\bar{\text{H}}$ following the same procedure discussed in Sec.5.1.2. The efficiency $\times$ acceptance has been parametrized with a piecewise polynomial, in order to use it for the signal pdf correction. The efficiency $\times$ acceptance and the parameterization are shown in Fig.13. The correction for the absorption from material was included also in the efficiency $\times$ acceptance evaluation, following the same procedure described and used in Sec.5.1.2. First $N^{\text{rec}}(p_{\text{T}}$ and ct) was computed, obtaining a 2D histogram p_{T} and ct. Then the entries of each bin were corrected with the probability (orange histogram in Fig.16) of the corresponding p_{T} bin, $N^{\text{rec}}(p_{\text{T}}, c\text{t}) \cdot p_{Observe_{^{3}_{\Lambda}\text{H}}}(p_{\text{T}})$. Finally the efficiency $\times$ acceptance was evaluated using the for N^{rec} the distribution obtained from the projection on the ct axis of TH2F previously corrected for the absorption.

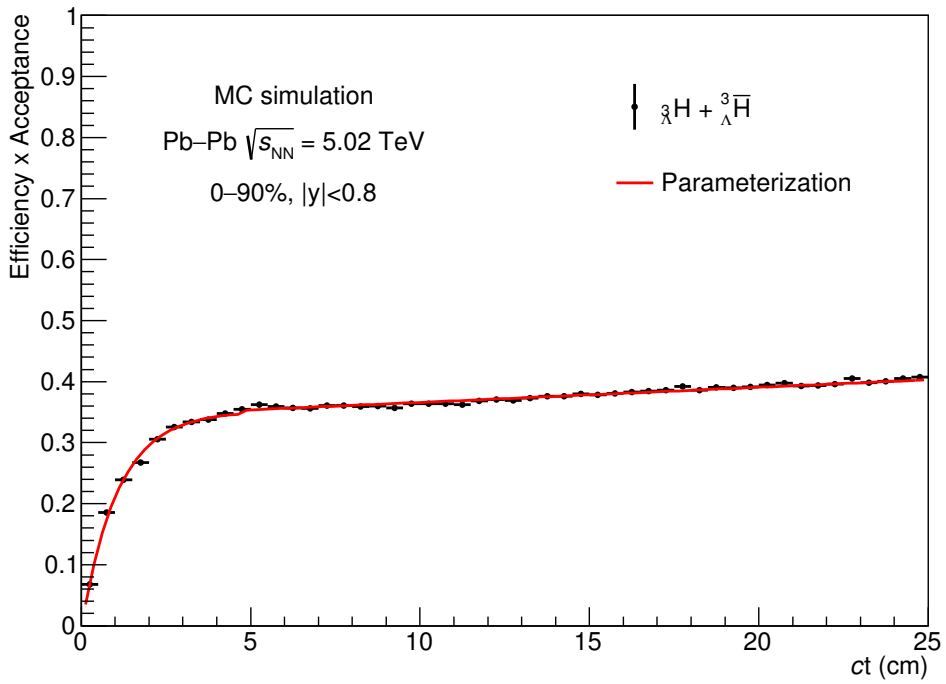

Fig. 13: Efficiency × acceptance vs ct for $^{3}_{\Lambda}$H + $^{3}_{\Lambda}\overline{\text{H}}$ (black) with superimposed the piecewise polynomial parameterization (red line), used for the correction.

Thus, the corrected pdf used for the signal is:

$$pdf_{signal}^{corrected} = pdf_{signal} \cdot (efficiency \times acceptance) \tag{16}$$

After tuning the background pdfs (Sec.5.2.2) and correcting the signal exponential pdf, a fit to the ct distribution in the signal range was performed, with the maximum-likelihood option, to extract the lifetime τ of the hypertriton. The statistical uncertainty was evaluated with log-likelihood ratio and a confidence interval of 68.3%.

The result from this method, shown in Fig.14, is:

$$c\tau = 7.20^{+1.20}_{-0.93}(stat.)\ cm \tag{17}$$

$$\tau = 240^{+40}_{-31}(stat.)\ ps \tag{18}$$

6 Absorption

Geant3 does not take into account any interaction of $^{3}_{\Lambda}$H and $^{3}_{\Lambda}\overline{\text{H}}$ with the material and this is shown in Fig.8, where the efficiency for $^{3}_{\Lambda}$H is close to the one of $^{3}_{\Lambda}\overline{\text{H}}$. In order to estimate the absorption of the $^{3}_{\Lambda}$H the same procedure used in the previous analysis [1] has been adopted. Since the cross section for (anti-)nuclei is barely unknown and the data for the (anti-)hypernuclei are totally missing, the starting point for this study was the absorption of (anti-)protons.

Fig.15 shows the fraction of protons (red) and anti-protons (blue) which do not reach the TPC and these fractions were obtained using Geant3 and applying the Geant-Fluka correction. Following what

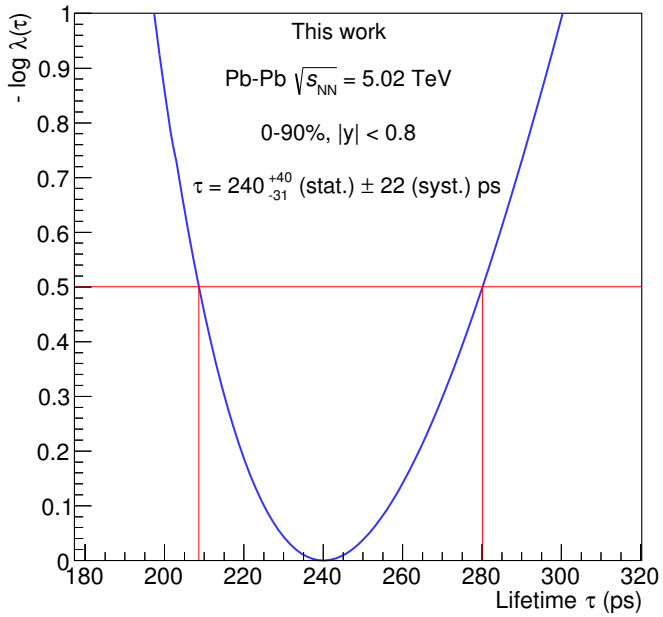

Fig. 14: Lifetime τ obtained from a maximum-likelihood fit to the ct distribution in the signal range. Statistical uncertainty are evaluated with log-likelihood ratio.

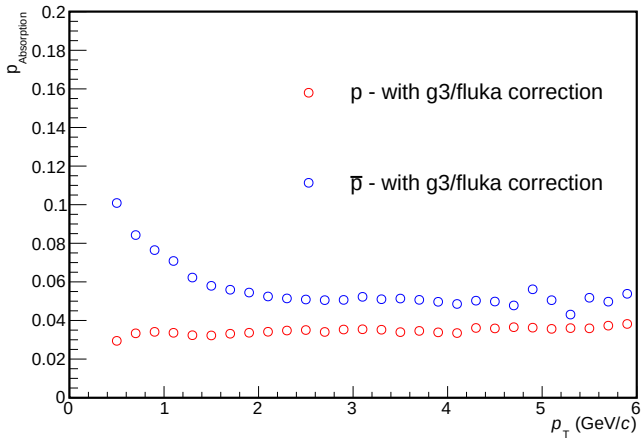

Fig. 15: Fraction of protons (red) and anti-protons (blue) which do not reach the TPC as a function of p_{T}. These values have been evaluated using Geant3 and applying the Geant3/Fluka correction.

previously done in [1], each bin in the histogram is the probability of a proton, with the corresponding p_{T}, to be absorbed ($p_{Absorption}$) and this probability can be written as:

$$p_{Absorption} = 1 - e^{-n_0 \sigma L}. \tag{19}$$

where n_0 is the number of scattering center of the target, σ is the cross-section of the projectile on the target and L is the path of the projectile.

In order to evaluate the probability to observe a ${}^{3}_{\Lambda}\mathrm{H}$ ($p_{Observe_{{}^{3}_{\Lambda}\mathrm{H}}}$), the absorption probability of the ${}^{3}_{\Lambda}\mathrm{H}$ ($p_{Absorption_{{}^{3}_{\Lambda}\mathrm{H}}}$) and the absorption probability of the ${}^{3}\mathrm{He}$ ($p_{Absorption_{{}^{3}\mathrm{He}}}$) were needed.

As previously mentioned, the cross-section for (anti-)nuclei is barely known and, since one of the ${}^{3}_{\Lambda}$H daughters is a ^{3}He, the $p_{Absorption}$ of the ^{3}He has been evaluated starting from the one of the proton and considering the ^{3}He as a cluster of 3 nucleons:

$$p_{Absorption_{^3\mathrm{He}}} = 1 - p^3_{NotAbsorption_p}. \tag{20}$$

The evaluation of the $p_{Absorption}$ of the ${}^{3}_{\Lambda}$H was done following the same procedure, but, since the hypertriton is barely bound (Λ binding energy B_Λ =130 keV), the cross-section was increased by 50%

$$p_{Absorption_{{}^{3}_{\Lambda}\mathrm{H}}} = 1 - e^{-1.5 n_0 \sigma_{^3\mathrm{He}} L}. \tag{21}$$

These probabilities were used to evaluate the probability not to observe a ${}^{3}_{\Lambda}$H:

$$p^{(PV-TPC)}_{NotObserve_{{}^{3}_{\Lambda}\mathrm{H}}} = p^{(PV-SV)}_{Absorption_{{}^{3}_{\Lambda}\mathrm{H}}} + \left(1 - p^{(PV-SV)}_{Absorption_{{}^{3}_{\Lambda}\mathrm{H}}}\right) \cdot p^{(SV-TPC)}_{Absorption_{^3\mathrm{He}}}. \tag{22}$$

where (PV-SV) is the distance between primary and secondary vertex, while (SV-TPC) is the distance between the secondary vertex and the TPC inner wall. Finally it was possible to compute the correction as:

$$p^{(PV-TPC)}_{Observe_{{}^{3}_{\Lambda}\mathrm{H}}} = \left(1 - p^{(PV-TPC)}_{NotObserve_{{}^{3}_{\Lambda}\mathrm{H}}}\right) \tag{23}$$

This probability was evaluated for different distances between primary and secondary vertex and two limiting cases are shown in Fig.16: the black curves correspond to a ${}^{3}_{\Lambda}$H which decays inside the beam pipe, so the $p_{NotObserve_{{}^{3}_{\Lambda}\mathrm{H}}}$ corresponds to the $p_{Absorption_{^3\mathrm{He}}}$, while the blue curve corresponds to a ${}^{3}_{\Lambda}$H which travels without decaying through the whole ITS. In order to assess the absorption, the mean value between the two limiting cases has been evaluated.

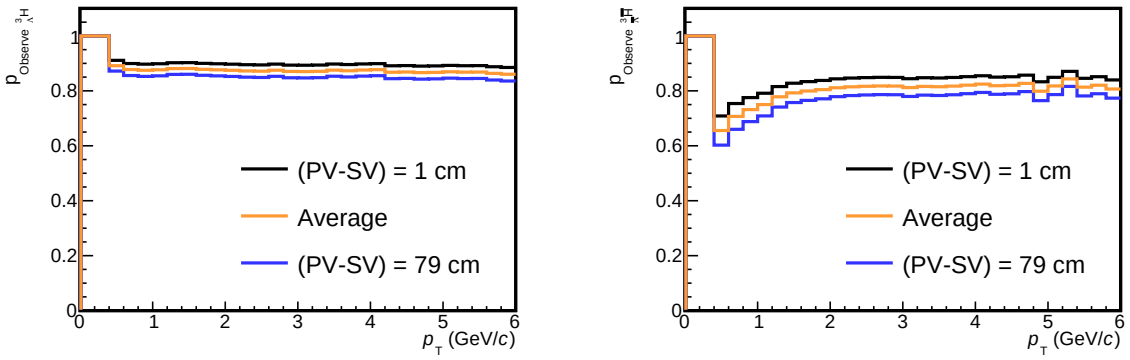

Fig. 16: $p_{Observe}$ ${}^{3}_{\Lambda}$H (left) and ${}^{3}_{\bar{\Lambda}}\overline{\mathrm{H}}$ (right) as a function of p_{T} for two limiting case: ${}^{3}_{\Lambda}$H(${}^{3}_{\bar{\Lambda}}\overline{\mathrm{H}}$) decays inside the beam pipe (black curve) or close to the TPC (blue curve). The average between the two limiting case (orange curve) is used as correction for the absorption.

7 Systematic uncertainties

In the systematic uncertainty evaluation all the possible systematic uncertaintiy sources should be considered and the total uncertainty can be assessed as the sum in quadrature of the maximum ΔY /Y for each source. For each of these selection variation the analysis was repeated from the beginning. Changing the selection criteria, implies a variation in the sample of (${}^{3}_{\bar{\Lambda}}\overline{\mathrm{H}}$)${}^{3}_{\Lambda}$H candidates analysed. The low statistics,

present in this analysis, can lead to a variation in the results, ΔY, which is dominated by the statistical component and, in this way, the statistical uncertainty can dominate the systematic uncertainty. Only the statistically significant variations of the final results were kept into account in the systematic uncertainty.

In order to disentangle the systematic uncertainty from the statistical one, the, so-called, "*Barlow criterion*", from Roger Barlow's paper [5], was used.

According to this criterion, if we have two estimates of a physical quantity, $\mathbf{x}_1$ and $\mathbf{x}_2$, with statistical uncertainty σ_1 and σ_2 respectively, obtained with a variation of the selection criteria (e.g topological cuts, PID), the two statistical uncertaintyies are strongly correlated because they share almost the same statistics. A way to check if the difference $\Delta = x_1 - x_2$ is statistically significant is to compare it for the $\sigma_{\Delta Y}$, which means to evaluate the variation, with respect to the nominal selection, in number of σ. In case of sub-samples with different statistics, it can be measured as:

$$\sigma_\Delta = \sqrt{|\sigma_1^2 - \sigma_2^2|} \tag{24}$$

and then compute the number of σ for this variation as:

$$\Delta/\sigma_\Delta \tag{25}$$

The criterion suggests to accept a variation as systematic uncertainty only if the ratio $|\Delta/\sigma_\Delta|$ is larger than 3 (or 2 to be more conservative), in order to understand if the applied variations are significant and they can be accounted as systematic uncertainties. In this analysis it was decided to be more conservative and to consider as systematic uncertainty, those variations larger than 2. If the criterion is satisfied the variation is accounted as systematic uncertainty.

7.1 Lifetime - "corrected *c*t spectra" method

Possible sources of systematics uncertainty for the "corrected *c*t spectra" method are:

- Topological cuts
- Particle Identification
- Material budget
- Single track efficiency
- Absorption from material

The systematics, which passed the Barlow criterion, were evaluated performing again all the analysis steps and measuring the variation on the lifetime value τ from the one obtained with the nominal selections. In the following the details on the study of the different source of systematics are reported.

7.1.1 Topological cuts

The cuts used for the candidates selection (i.e. $\cos(\theta_{pointing})$, DCA_{tracks} and $p_{\mathrm{T}}^{^3\mathrm{He}}$) were varied and in Table 8 the different set of trials are reported.

Fig.17 (*Left*) shows the variation induced on the lifetime value (ΔY) and normalized to the reference value (Y) obtained with the nominal selections of Table 6. The first bin has ΔY/Y equal to zero because Set 0 corresponds to the nominal selections and is used as reference in the normalization of the following bins (Set1-8). On the other side, Fig.17 (*Right*) shows the number of σ, evaluated accordingly to Eq.25, for each set of cuts and none of the investigated topological cuts is statistically relevant, following the Barlow's recipe. The dashed lines on Fig.17 (*Right*) represents the threshold on $|\Delta/\sigma_\Delta|$ applied in this analysis in order to accept/reject a variation as systematic uncertainty.

	Set 0	*Set 1*	*Set 2*	*Set 3*	*Set 4*	*Set 5*	*Set 6*	*Set 7*	*Set 8*
$p_{\mathrm{T}}^{^3\mathrm{He}}$	1.8	1.8	1.8	1.6	1.6	1.6	1.9	1.9	1.9
DCA_{tracks}	0.7	0.5	0.8	0.7	0.5	0.8	0.5	0.7	0.8
$\cos(\theta_{pointing})$	0.995	0.997	0.992	0.992	0.997	0.992	0.995	0.997	0.992

Table 8: Different sets of cuts used to study the systematics from candidates selection criteria

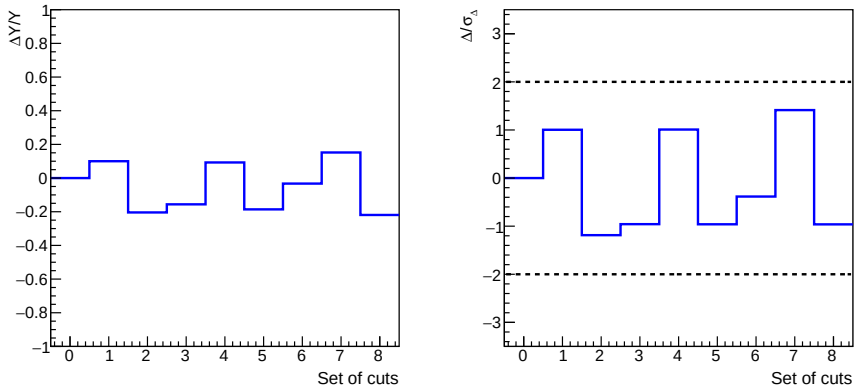

Fig. 17: (*Left*)ΔY/Y for each set of cuts. The reference value (*Set 0*) corresponds to the set of cuts used in the analysis. (*Right*) Δ/σ_Δ for each set of cuts. The black dashed lines are the selection applied to accept the variation as systematic uncertainty.

7.1.2 Particle Identification

The number of σs used to identify the ^{3}He and the π was varied in order to understand if the effect of such variations could lead to a systematic uncertainty on the lifetime determination. In Table 9 the different PID selections used for this study are reported.

	Set 0	*Set 1*	*Set 2*	*Set 3*	*Set 4*	*Set 5*	*Set 6*	*Set 7*	*Set 8*
$\lvert n\sigma_\pi \rvert$	3	2	2	2	2	2	2	3	3
$\lvert n\sigma_{^3\mathrm{He}} \rvert$	3	3	3	2.5	2	2	4	4	4
$n\sigma_{triton}$	0	0	3	3	3	6	6	6	3

Table 9: Different sets of number of σs used to identify the $^3_\Lambda$H daughters

Fig.18 (*Left*) shows the ΔY/Y, previously defined, for different set of nσ selection for the daughters identification. Fig.18 (*Right*) shows the Δ/σ_Δ for each variation of the particle identification selection. As already mentioned in Sec.7.1.1, the Set 0 corresponds to the nominal selection applied in this analysis. The distribution in Fig.18 (*Right*), shows that some differences are within the 2σ band, so, for this reason, the variations, induced from changing the PID requirements, are not considered in the systematic evaluation.

7.1.3 Material budget

The material budget is described in ALICE simulation with a good approximation. However it was important to investigate possible discrepancies in the evaluated reconstruction efficiency related to the material budget description. Then two additional MC sample were produced, varying the material budget used in the simulation. The material budget variation has been chosen taking into account the uncertainty on its determination and this was driven by the results obtained from the photon conversion analyses [6]. This analysis lead to a symmetric uncertainty on the material budget of $\pm$ 4.5% and this variation is used in the two MC samples. The two MC samples, used for the study of the systematics due to the material budget, are *LHC17d5a* (+4.5% material budget) and *LHC17d5b* (-4.5% material budget), where

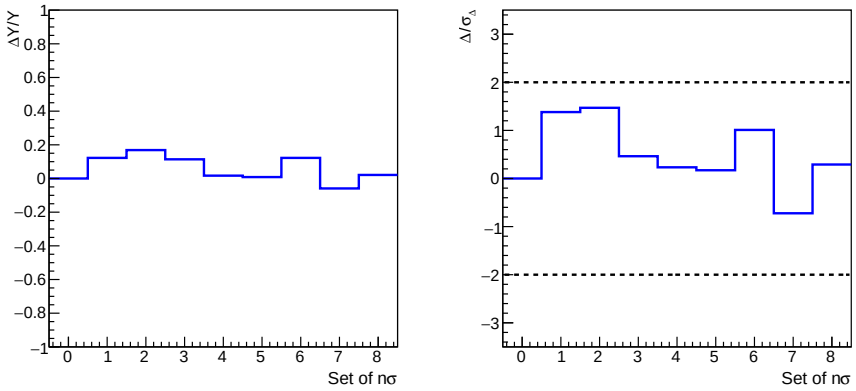

Fig. 18: (*Left*)ΔY/Y for each set of PID selection criteria. The reference value (*Set 0*) corresponds to the PID selection used in the analysis. (*Right*) Δ/σ_Δ for each set of PID selection criteria. The black dashed lines are the selection applied to accept the variation as systematic uncertainty.

the simulation configuration is the same used for *LHC16h7*{*a,b,c*}. More details on this MC productions can be found in [7].

The efficiency × acceptance was recomputed using these two MC productions and the results are shown in Fig.19. It is possible to see a clear trend with the material budget with higher efficiency (blue markers) with reduced material budget and lower efficiency (red markers) with increased material budget. This is, somehow, expected since with increased material budget the particle lose more energy while traversing the material, while the opposite behaviour is foreseen with decreased material budget.

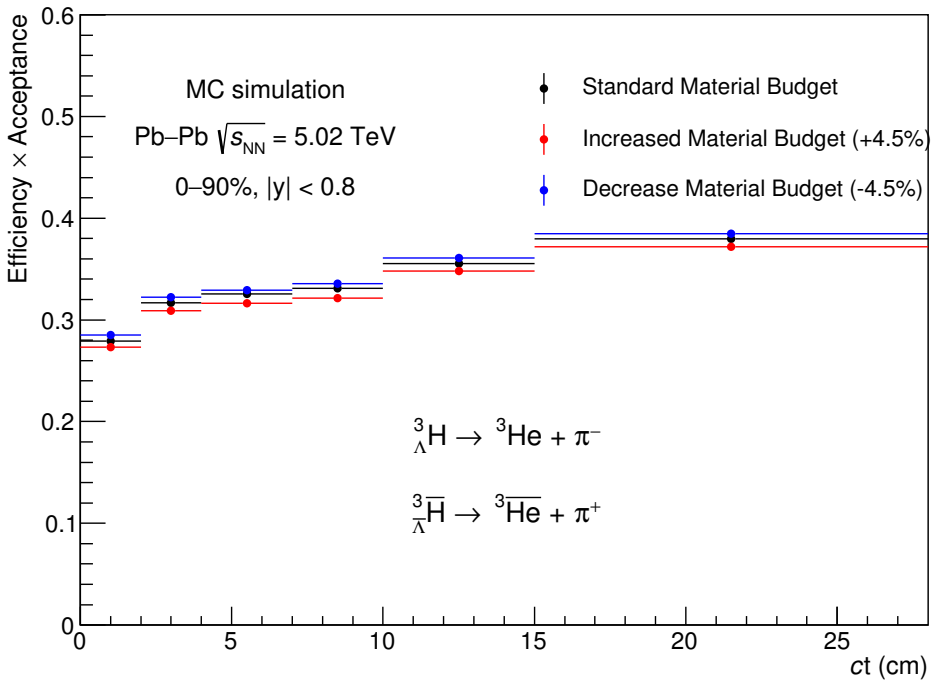

Fig. 19: Efficiency × acceptance vs *c*t for ${}^3_\Lambda\mathrm{H}$ + ${}^3_{\overline{\Lambda}}\overline{\mathrm{H}}$ with nominal (black), increased (red) and decreased (blue) material budget. The same bins adopted for the yields extraction are used.

For each *c*t bin analysed, the variations of the efficiency × acceptance, induced by the change of the ma-

terial budget used in the simulation, are supposed to follow a uniform distribution around the efficiency × acceptance with nominal material budget (black markers). For this reason the systematic uncertainty due to material budget is evaluated as:

$$\sigma_{Mat.Budget}(ct) = \frac{\varepsilon_{max} - \varepsilon_{min}}{\sqrt{12}} \tag{26}$$

In the ct region used for this analysis, the systematic from material budget lies between 4‰ and 6‰. The last value of 6‰ was assigned as systematic uncertainty.

7.1.4 Single track efficiency

From the analysis of the "*Transverse momentum spectra and nuclear modification factor for charged hadrons in Pb–Pbcollisions at* $\sqrt{s_{\rm NN}}$ *= 5.02 TeV*" analysis: Single track efficiency = 3.5% [8]

7.1.5 Absorption from material

Two main sources of systematics uncertainty have been investigated for the absorption from material:

- average correction
- $^{3}_{\Lambda}$H cross-section

As described in Sec.6, the probability to observe an $^{3}_{\Lambda}\mathrm{H}\,^{3}_{\Lambda}\overline{\mathrm{H}}$ is the average between two extreme cases: the probability to observe an $^{3}_{\Lambda}$H which decays in the beam pipe (PV-SV = 1 cm) and the probability to observe an $^{3}_{\Lambda}$H which decays close to the TPC (PV-SV = 79 cm). The systematic from this assumption was evaluated using the probabilities of the two extreme cases, instead of the average. The efficiency × acceptance was evaluated in the two different cases and the systematics uncertainty has been assigned as the semi-difference between the efficiencies in the two extreme cases. As can be seen in Fig.20 the semi-difference lead to an uncertainty of 3.5%

The other source of systematic uncertainty is the $^{3}_{\Lambda}$H cross-section, which is obtained increasing the one of the ^{3}He by a 50%, as Sec.6. In this case the systematics was obtained varying the scaling factor used for the cross-section. This scaling factor was reduced ($\sigma_{^{3}_{\Lambda}\mathrm{H}} = 1\cdot\sigma_{^{3}\mathrm{He}}$) and increased ($\sigma_{^{3}_{\Lambda}\mathrm{H}} = 2\cdot\sigma_{^{3}\mathrm{He}}$) and the correction for absorption was computed for both the configuration. Then the efficiencies were evaluated in the two cases and the semi-difference was computed, leading to a 3.4% of uncertainty as shown in Fig.21. At last, the two uncertainty have been summed in quadrature in order to assess the systematics uncertainty for the absorption of 5%.

7.2 Lifetime - "unbinned fit" method

Possible sources of systematics uncertainty for the "unbinned fit" method are:

- Topological cuts (procedure details in Sec.7.1.1)
- Particle Identification (procedure details in Sec.7.1.2)
- Material budget (procedure details in Sec.7.1.3)
- Single track efficiency
- Absorption from material

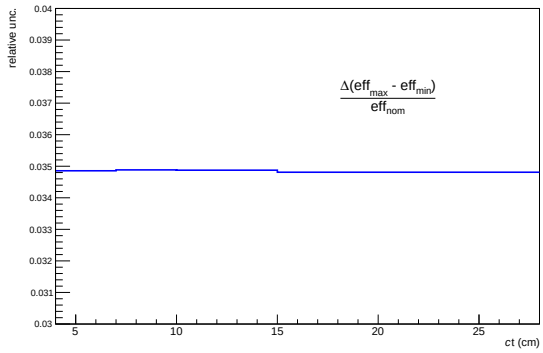

Fig. 20: Systematic uncertainty from correction with extreme cases (PV-SV = 1cm, 79cm)

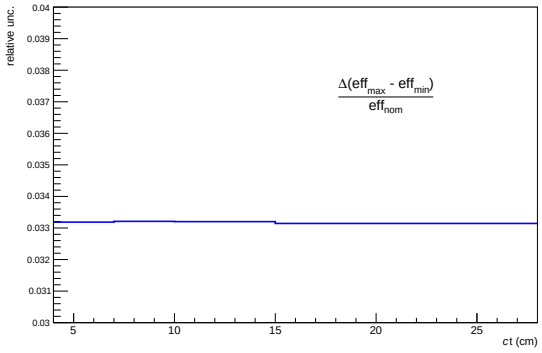

Fig. 21: Systematic uncertainty from variation of $\sigma_{^3He}$ rescaling

The systematics uncertainties, related to this method, were studied and evaluated with the same procedure described in Sec.7.1. a detailed description of the procedure used to evaluate each systematics uncertainty can be found in the previous section and the correct reference is also reported in the list above. Only the results of the study and the accounted systematics are reported in the following.

7.2.1 Topological cuts

The cuts used for the candidates selection (i.e. $\cos(\theta_{pointing})$, DCA_{tracks} and $p_{\text{T}}^{^3\text{He}}$) were varied and in Table 10 the different set of trials are reported.

	Set 0	*Set 1*	*Set 2*	*Set 3*	*Set 4*	*Set 5*	*Set 6*	*Set 7*	*Set 8*
$p_{\text{T}}^{^3\text{He}}$	1.8	1.8	1.8	1.6	1.6	1.6	1.9	1.9	1.9
DCA_{tracks}	0.7	0.5	0.8	0.7	0.5	0.8	0.5	0.7	0.8
$\cos(\theta_{pointing})$	0.995	0.997	0.992	0.992	0.997	0.992	0.995	0.997	0.992

Table 10: Different sets of cuts used to study the systematics from candidates selection criteria

Fig. 22 (*Left*) shows the relative variation (ΔY/Y) induced on the lifetime value with respect to reference value obtained with the nominal selections of Table 6. The first bin has ΔY/Y equal to zero because Set 0 corresponds to the nomial selections and is used as reference in the normalization of the following bins (Set1-8). On the other side, Fig. 22 (*Right*) shows the Δ / σ_Δ for each set cuts and none of the investigated topological cuts is statistically relevant, following Barlow's recipe. The dashed lines on Fig. 22 (*Right*) represents the threshold on $|\Delta/\sigma_\Delta|$ applied in this analysis in order to accept/reject a variation as systematic uncertainty.

7.2.2 Particle Identification

The number of σs used to identify the ^{3}He and the π was varied as previously done and the different PID selections are reported in Table 11.

	Set 0	*Set 1*	*Set 2*	*Set 3*	*Set 4*	*Set 5*	*Set 6*	*Set 7*	*Set 8*
$\lvert n\sigma_\pi \rvert$	3	2	2	2	2	2	2	3	3
$\lvert n\sigma_{^3\text{He}} \rvert$	3	3	3	2.5	2	2	4	4	4
$n\sigma_{triton}$	0	0	3	3	3	6	6	6	3

Table 11: Different sets of number of σs used to identify the $^3_\Lambda$H daughters

Fig.23 (*Left*) shows the ΔY/Y, previously defined, for different set of nσ selection for the daughters identification. Fig.23 (*Right*) shows the Δ/σ_Δ for each variation of the particle identification selection.

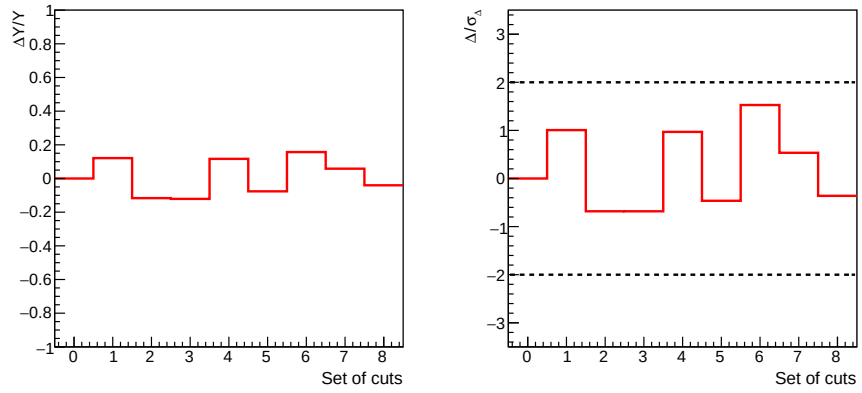

Fig. 22: (*Left*)ΔY/Y for each set of cuts. The reference value (*Set 0*) corresponds to the set of cuts used in the analysis. (*Right*) Δ/σ_Δ for each set of cuts. The black dashed lines are the selection applied to accept the variation as systematic uncertainty.

As already mentioned in Sec.7.1.1, the Set 0 corresponds to the nominal selection applied in this analysis. In this case the variation induced by changing the requirements for the daughters identification are lower than 2σ, as can be observed in Fig.23 (*Right*), and for this reason these variations are not considered as systematics uncertainty, accordingly to the Barlow criterion .

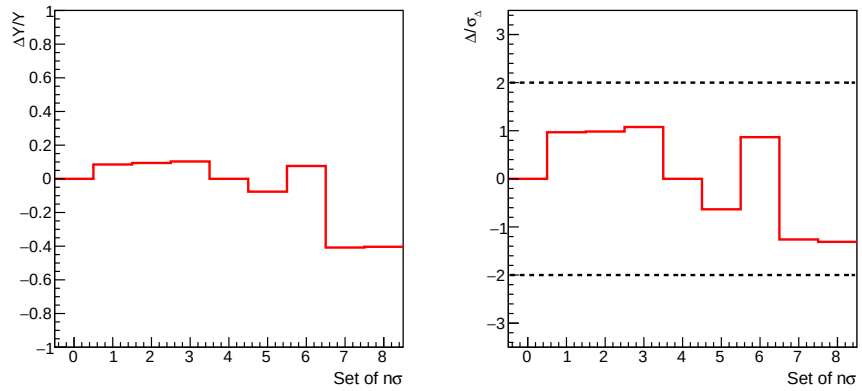

Fig. 23: (*Left*)ΔY/Y for each set of PID selection criteria. The reference value (*Set 0*) corresponds to the PID selections used in the analysis. (*Right*) Δ/σ_Δ for each set of PID selection criteria. The black dashed lines are the selection applied to accept the variation as systematic uncertainty.

7.2.3 Material budget

Accordingly to the procedure described in Sec.7.1.3, the efficienci $\times$ acceptance was evaluated using two MC productions, one with increased (*LHC17d5a*) and one with reduced (*LHC17d5b*) material budget. The efficiencies were computed with the same binnings used for the nominal one and the results are shown in Fig.24. At a first glance, it is possible to see a trend in the efficiency with the material budget. The efficiency is higher (blue markers) with reduced material budget and lower (red markers) with increased material budget, compared to the one with nominal material budget (black marker). Since the variations of the efficiency $\times$ acceptance, induced by the change of the material budget, are supposed to follow a uniform distribution, the uncertainty is assigned accordingly to Eq. 26, which is the standard deviation of a uniform distribution.

In the ct region used for this analysis, the systematic uncertainty due to the material budget lies between 4‰ and 7‰. A 7‰ was assigned as systematic uncertainty for the material budget.

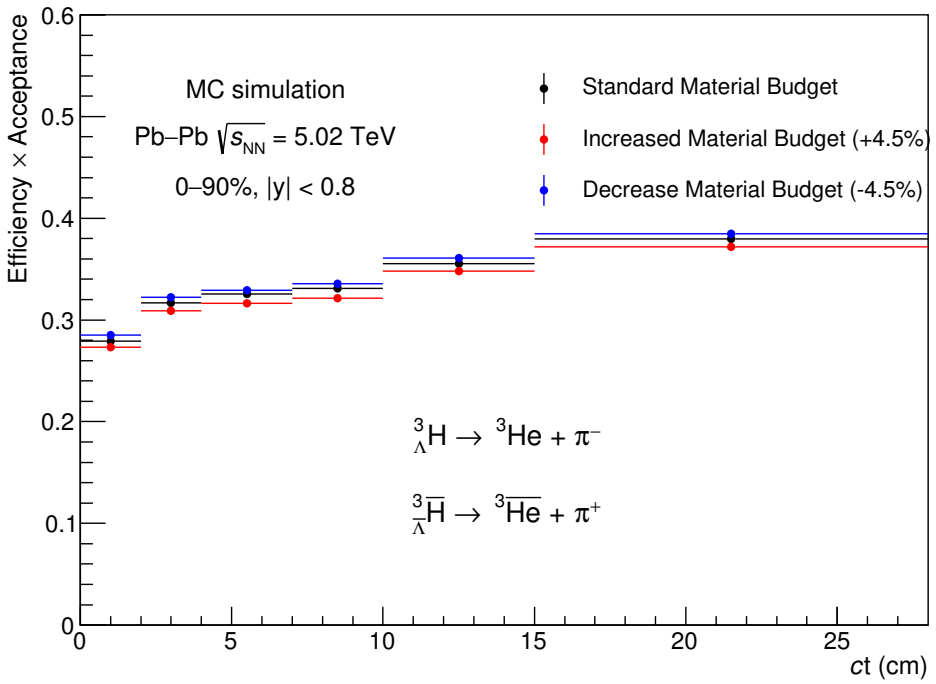

Fig. 24: Efficiency × acceptance vs ct for $^{3}_{\Lambda}$H + $^{3}_{\bar{\Lambda}}\bar{\text{H}}$ with nominal (black), increased (red) and decreased (blue) material budget. The same bins adopted for the yields extraction are used.

7.2.4 Single track efficiency

From the analysis of the "*Transverse momentum spectra and nuclear modification factor for charged hadrons in Pb–Pbcollisions at* $\sqrt{s_{\text{NN}}}$ = *5.02 TeV*" analysis: Single track efficiency = 3.5% [8]

7.2.5 Absorption from material

The same sources of systematics uncertainties described in Sec.7.1.5 have been investigated also for the second method. The absorption correction was varied as previously done: in one case taking the absorption correction for the two extreme cases (PV-SV = 1cm and PV-SV = 79cm) and in the other case varying the scale factor used for the $\sigma_{^{3}_{\Lambda}\text{H}}$. Also in this case, the systematics uncertainties were evaluated with the semi-difference between the efficiencies obtained after the application of the correction for absorption. Fig.25 shows the semi-difference of the efficiencies obtained using the correction for the extreme cases (PV-SV = 1cm, 79cm) and normalized to the nominal efficiency. It is evaluated as a function of ct and the trend is almost flat, leading to an uncertainty of 3.5%.

Fig.26 shows the semi-difference as a function of ct of the efficiencies evaluated after varying the scaling factor used to obtain the $\sigma_{^{3}_{\Lambda}\text{H}}$ cross-section. Also in this figure the trend of this uncertainty is flat and it was decided to assign a 3.4% of systematics uncertainty.

As previously done, the two systematics have been summed in quadrature to assess the systematic uncertainty for absorption from material, which is of 5%.

7.3 Summary of the systematic uncertainty

The systematics uncertainty evaluated for the lifetime estimate with the "corrected ct spectra" method are listed in Table 12.

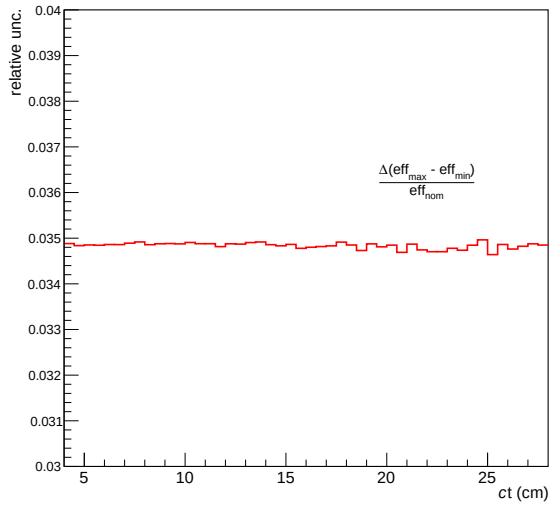

Fig. 25: Systematic uncertainty from correction with extreme cases (PV-SV = 1cm, 79cm)

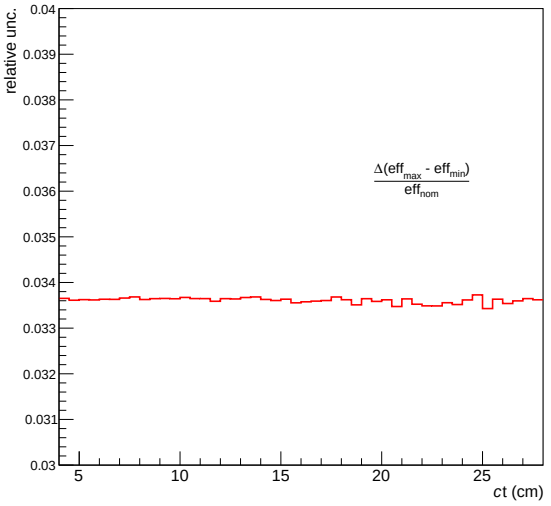

Fig. 26: Systematic uncertainty from variation of $\sigma_{^3He}$ rescaling

Systematics "corrected *c*t spectra" method	
Contribution	value
Topological cuts	Not possible to disentangle syst. from stat. uncertainty
Particle Identification	Not possible to disentangle syst. from stat. uncertainty
Material budget	0.6%
Single track efficiency	7% (3.5%$\times$ 2 tracks)
Absorption from material	5%
Total	9%

Table 12: Summary of systematics uncertainty on the lifetime estimated with the "corrected *c*t spectra" method

The systematics uncertainty evaluated for the lifetime estimate with the "unbinned fit" method are listed in Table 13.

Systematics "unbinned fit" method	
Contribution	value
Topological cuts	Not possible to disentangle syst. from stat. uncertainty
Particle Identification	Not possible to disentangle syst. from stat. uncertainty
Material budget	0.7%
Single track efficiency	7% (3.5%$\times$ 2 tracks)
Absorption from material	5%
Total	9%

Table 13: Summary of systematics uncertainty on the lifetime estimated with the "unbinned fit" method

8 Results

The results on the lifetime obtained with the two method are:

- **Method "corrected *c*t spectra"**

$$c\tau = 7.25^{+1.02}_{-1.13}(stat.) \pm 0.59(syst.)\ cm \tag{27}$$

$$\tau = 242^{+34}_{-38}(stat.) \pm 20(syst.)\ ps \tag{28}$$

- **Method "unbinned fit"**

$$c\tau = 7.20^{+1.20}_{-0.93}(stat.) \pm 0.66(syst.)\ cm \tag{29}$$

$$\tau = 240^{+40}_{-31}(stat.) \pm 22(syst.)\ ps \tag{30}$$

9 Performance: ${}^{3}_{\Lambda}\mathrm{H}$ and ${}^{3}_{\bar{\Lambda}}\overline{\mathrm{H}}$ 3 body decay

This section is written in order to introduce the data sample and the selections used to obtain the invariant mass plot for the ${}^{3}_{\Lambda}\mathrm{H}$ and ${}^{3}_{\bar{\Lambda}}\overline{\mathrm{H}}$ from the 3 body decay channel. These plots will be presented at the Physics Forum for a Perfomance Plot request.

References

[1] ALICE Collaboration, *Phys. Lett.* B **754** (2016) 360-372

[2] `https://github.com/alisw/AliDPG/`

[3] ALICE Collaboration, *Int. J. Mod. Phys.* A **29** (2014) 1430044

[4] D.H. Davis, *Nucl. Phys.* A **754** (2005) 3-13

[5] R. Barlow, *Advanced Statistical Techniques in Particle Physics*, Proceedings, Conference, Durham, UK, March 18-22, 2002, pp. 134144, 2002

[6] ALICE Collaboration, https://aliceinfo.cern.ch/ArtSubmission/node/120

[7] https://alice.its.cern.ch/jira/browse/ALIROOT-7205

[8] ALICE Analysis Note, https://aliceinfo.cern.ch/Notes/node/473